

The Convex Relaxation Method on Deconvolution Model with Multiplicative Noise

Yumei Huang¹, Michael Ng² and Tiejong Zeng^{2,*}

¹ School of Mathematics and Statistics, Lanzhou University, Lanzhou 730000, China.

² Department of Mathematics, Hong Kong Baptist University, Kowloon Tong, Hong Kong.

Received 31 August 2011; Accepted (in revised version) 9 March 2012

Available online 21 September 2012

Abstract. In this paper, we consider variational approaches to handle the multiplicative noise removal and deblurring problem. Based on rather reasonable physical blurring-noisy assumptions, we derive a new variational model for this issue. After the study of the basic properties, we propose to approximate it by a convex relaxation model which is a balance between the previous non-convex model and a convex model. The relaxed model is solved by an alternating minimization approach. Numerical examples are presented to illustrate the effectiveness and efficiency of the proposed method.

AMS subject classifications: 52A40, 65K10, 65K15, 90C26

Key words: Alternating minimization, convergence, deblurring, multiplicative noise, non-convex model.

1 Introduction

The electromagnetic field is a physical field emitted by electrically charged objects and which impacts the properties of charged objects in the neighborhood of the field. Visible light is the electromagnetic field in certain range of frequencies. The electromagnetic field always bears important information of the charged objects generating it. This is the starting point of imaging formation. However, as the propagation of wave field usually suffers modest blurring, the loss of information seems to be unavoidable. Moreover, the observed field can be further affected by noise due to many known or unknown factors. In real applications, similar problems always exist. For instance, the photos of space targets produced by astronomical telescopes are often blurred by atmospheric

*Corresponding author. *Email address:* zeng@hkbu.edu.hk (T. Zeng)

turbulence. In these regards, image blur and noise are fundamental problems in the domain of image processing and they continue to attract the attention of researchers.

Evidently, the deblurring process under noise is not well-posed in the sense of Hadamard [13]. The observed blurred and noisy image only provides partial restrictions on the solution image. There exist various candidature images which can match the observed degraded image under the given blur operator. Hence, the greatest challenge in deblurring and denoising is to design methods for restoring solutions toward more reasonable results adaptive to certain prior information [19].

In order to reconstruct the image, we need a mathematical description to show how the noisy and blurry image is formed. If that is not available, there are many algorithms to estimate the blur though it is beyond the scope of the current papers. In literatures, one usually supposes that the degraded image f is formed as:

$$f = Hw + v, \quad (1.1)$$

here f , w and v are an mn -by-1 vector corresponding to an m -by- n image, and they are observed image, original image and additive noise respectively. And the matrix $H \in \mathbb{R}^{mn \times mn}$ is the blur operator. Without loss of generality, here we assume that $H \geq 0$ holds in component-wise meaning.

Under this additive noise scheme, various approaches have been studied to handle the inverse problem (1.1). Among them, regularization methods which propose to find a solution image satisfying the previous mentioned prior information seem to be rather appealing. Many regularization techniques are established by least-square methods. As the number of unknowns concerned might be huge, these approaches are commonly iterative in nature. In the past decades, the total variation (TV) regularization functional has become popular since it can efficiently reserve sharp edges of images, see [1, 3, 8, 22, 27, 28]. This type of algorithm minimizes a functional composing of two different terms. One term is restricted on the blur operator and the other term corresponds to the TV regularization for the solution image.

Note that there have been a great deal of deblurring approaches in literatures devoting to removing the additive noise. In recent years, in a different discipline, much attention also has been paid increasingly to many other kinds of random noises. Such noises include multiplicative noise, see for instance [2, 5, 14, 21]; impulse noise and Poisson noise etc., see for instance [4, 6, 7, 15, 26] and [9, 20]. In this paper, we focus on the deblurring issues under the multiplicative noise.

The image reconstruction problem under multiplicative noise is evidently challenging since this kind of noise contaminates images in a totally different way from additive noise. That is, the observed image f is supposed to be the multiplication of the blurred image Hw and the noise v :

$$f = Hwv, \quad (1.2)$$

where again, H is the blur operator and w is the clean image. Note that here the noise v could follow different statistics such as Gaussian, Gamma or other distributions. Without

loss of generality, we assume that all the entries of w , v and f are positive. Due to this degraded mechanism, most of the information in the original image might be distorted seriously by multiplicative noise and the blur operator. The practical applications of multiplicative noise models are numerous [21]. For example, the models of coherent imaging systems, such as synthetic aperture radar (SAR), ultrasound imaging and laser images, are of multiplicative nature [5].

In literatures, for the simplest case where $H = Id$, here Id denotes the identity matrix, several variational approaches have been proposed to handle the multiplicative noise removal problems. Among them, total variation based models (for instance, see [2, 21]) seem to be quite interesting since this idea has been adopted to maintain image edges in the recovered images as the same purpose in additive noise restorations. Recently, Shi and Osher [23] considered a noisy observation $g = \log f = \log w + \log v$, which is obtained by putting logarithm operation to both sides of the degradation model $f = wv$, here they only considered the denoising case. They derived a total variation minimization model for multiplicative noise removal problems. On the other hand, Aubert and Aujol [2] used maximum a posteriori (MAP) regularization approach and proposed a functional whose minimizer corresponds to the denoised image to be recovered in the multiplicative noise removal problem. In their papers, the Gamma noise with mean one is considered. Although their functional is not convex, they still proved that the existence of the minimizer and demonstrated the capability of their model by numerical examples. As neither of models in [2, 23] is convex, this poses serious numerical difficulties. In [14], Huang et al. studied a convex model strongly related to the model proposed in [2]. Numerical results have shown that this convex model can provide denoised images with higher SNRs and better visual qualities, independent of the initial guesses. However, it is open question to extend this technique to the deblurring case. In [5], a split-Bregman algorithm is presented to solve the model in [14] directly and it is quite numerically efficient. In [24], Steidl and Teuber considered another variational restoration model consisting of the so called *I-divergence* as data fitting term and the total variation regularization or nonlocal means as regularizer for removing multiplicative Gamma noise. In [12], the multiplicative noise removal problem is handled by using L^1 fidelity term on frame coefficients. The reported numerical results there clearly outperform the main alternative methods especially for images containing tricky geometrical structures.

However, as far as we know, there exist very few papers addressing the deblurring problem under multiplicative noise. Indeed, this becomes extremely hard when H is not identity operator since it brings other instable issues. In [21], Rudin, Lions and Osher proposed two approaches: RLO-I, II (see below). The numerical results there seem to be rather promising though in certain sense, it is somewhat limited. In [2], Aubert and Aujol had also extended their model to handle the deblurring problem.

In this paper, inspired by the pioneer works [2, 21], we study the deblurring issues under multiplicative noise. The outline of the paper is as follows. In Section 2, we briefly review the previous work of [2, 21]. In Section 3, based on a new mechanism of degraded image formation, we propose a new model for multiplicative noise removal and deblur-

ring. Some basic properties including the maximum principle are studied. In Section 4, we further propose a convex relaxation model. In Section 5, we show experimental results to demonstrate the quality of the deblurring images and the efficiency of the proposed method. Finally, concluding remarks are given in Section 6.

Comparing with previous works, our contributions are rather clear. First, we propose a Tikhonov regularization technique to obtain a separable variable model which is much easier to handle in practice. Second, we approximate the non-convex term invoked by the multiplicative noise in the model by a convex relaxation one. This reduces significantly the instable numerical problem. Third, an alternating minimization algorithm is given and the convergence of the method is guaranteed.

2 Related works

Let us briefly review the previous works in [2, 21] since they should be considered as starting point of our paper. Throughout the paper, for any image w , the notation $w \geq 0$ means that it is in the non-negative cone of \mathbb{R}^{mn} .

2.1 Aubert-Aujol model

Suppose that observed image f is given by (1.2) where v is of Gamma distribution with mean one. Note that, as pointed out in [21], this model has been treated in [10] by homomorphic filtering. In Aubert-Aujol (AA) model, their functional in the discrete setting can be described as follows:

$$\min_{w \geq 0} \sum_{i=1}^{mn} \left(\log([Hw]_i) + \frac{[f]_i}{[Hw]_i} \right) + \lambda \|w\|_{TV}, \tag{2.1}$$

where $\|w\|_{TV}$ is the total variation (TV) regularization term and λ is the regularization parameter which measures the trade off between the first term in (2.1) and a regularized solution of (2.1). The discrete gradient operator $\nabla: \mathbb{R}^{mn} \rightarrow \mathbb{R}^{mn}$ is defined by:

$$(\nabla w)_{j,k} = ((\nabla w)_{j,k}^x, (\nabla w)_{j,k}^y)^T$$

with

$$(\nabla w)_{j,k}^x = \begin{cases} w_{j+1,k} - w_{j,k}, & \text{if } j < n, \\ 0, & \text{if } j = n, \end{cases}$$

$$(\nabla w)_{j,k}^y = \begin{cases} w_{j,k+1} - w_{j,k}, & \text{if } k < n, \\ 0, & \text{if } k = n, \end{cases}$$

for $j = 1, \dots, m, k = 1, \dots, n$. Here $w_{j,k}$ refers to the $(jm+k)$ th entry of the vector w (it is the (j,k) th pixel location of the image). The discrete total variation of w is defined by

$$\|w\|_{TV} := \sum_{1 \leq j \leq m, 1 \leq k \leq n} |(\nabla w)_{j,k}|_2 = \sum_{1 \leq j \leq m, 1 \leq k \leq n} \sqrt{|(\nabla w)_{j,k}^x|^2 + |(\nabla w)_{j,k}^y|^2}.$$

Model (2.1) was solved by gradient method in [2].

2.2 Rudin-Lions-Osher model

2.2.1 RLO-I model

Rudin-Lions-Osher model is slightly different from Aubert-Aujol model. Assume again that the observed image f is obtained by (1.2) with v governed by multiplicative noise of mean 1 and standard variance θ , in [21], the RLO-I model is designed as a constrained optimization problem as follows:

$$\begin{aligned} \min_{w \geq 0} \quad & \|w\|_{TV}, \\ \text{subject to:} \quad & \sum_{i=1}^{mn} \frac{[f]_i}{[Hw]_i} = 1, \\ & \sum_{i=1}^{mn} \left(\frac{[f]_i}{[Hw]_i} - 1 \right)^2 = \theta^2. \end{aligned} \quad (2.2)$$

2.2.2 RLO-II model

Different from RLO-I model, here we assume that the observed image f is obtained via:

$$f = Hw + wv,$$

where again H is a convolution operator, v is Gaussian white noise with mean zero and standard variance θ .

The RLO-II model reads:

$$\begin{aligned} \min_{w \geq 0} \quad & \|w\|_{TV}, \\ \text{subject to:} \quad & \sum_{i=1}^{mn} \frac{[f - Hw]_i}{[w]_i} = 0, \\ & \sum_{i=1}^{mn} \left(\frac{[f - Hw]_i}{[w]_i} \right)^2 = \theta^2. \end{aligned} \quad (2.3)$$

In [21], both proposed models were solved by the gradient projection method.

Let us mention that as none of the above three models is convex, the gradient projection method may stick at some local minimizers and the restoration results strongly rely on the initial guesses and the numerical schemes. Moreover, as the blurring operator H also involves another instable problem, it is rather difficult to get a steady state of the above models in practice.

3 The proposed model

In order to handle the above difficulties, in this paper, we slightly modify the image formation mechanism to derive a separable model and then study its convex relaxation.

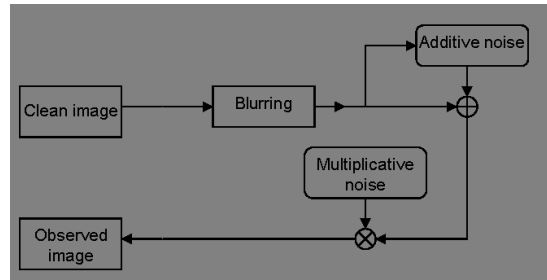


Figure 1: Physical imaging pipeline. After blurring and additive noise, the image is further degraded by multiplicative noise.

3.1 Imaging pipeline

As both the RLO-I model and AA model assume that $f = Hwv$. We also keep this as a basic pattern. Let us change it as:

$$f = (Hw + b)v, \tag{3.1}$$

where f, H, v are the same as in model (1.2) and b is Gaussian white noise with standard variance σ . In other words, here we suppose that Hw is also corrupted by some additive Gaussian noise. In fact, when $\sigma = 0$, the model (3.1) will become the usual multiplicative deblurring model (1.2). The imaging pipeline of (3.1) is illustrated in Fig. 1. After blurring and additive noise, the image is further degraded by multiplicative noise. The blurring could be caused by atmospheric attenuation or lens/geometric distortion, etc.; the additive noise should be regarded as syntheses of many factors such as fixed pattern noise, dark current noise, short noise or thermal noise (see [18,25]), etc. And the multiplicative noise is caused by multiplicative nature which is common in coherent imaging systems, such as synthetic aperture radar (SAR), ultrasound imaging and laser images. Overall, (3.1) could be regarded as an integration of the CCD camera imaging pipeline (see [18,25]) with multiplicative noise.

In order to make the new mechanism much near the original system, we can further assume that b is very small. Moreover, it is common assumption that $\inf f > 0$. Hence, we suppose that:

$$0 < \sigma \leq 2 \inf f.$$

The impact of right side of the above formula will be clarified later.

A MAP analysis on (3.1) suggests that we should consider the following model:

$$\min_{u > 0, w} \sum_{i=1}^{mn} \left(\log[u]_i + \frac{[f]_i}{[u]_i} \right) + \frac{\|Hw - u\|^2}{2\sigma^2} + \lambda\phi(w), \tag{3.2}$$

where u is an intermediate image, $\phi(w)$ is a convex regularization term. The unpleasant restriction that $u > 0$ (which is open) can be removed through the coming Proposition 3.3 (see below). Moreover, observing (3.2), we have another interpretation for (3.1). Indeed,

we introduce an extra Tikhonov regularization term for the blurring operator. This is helpful to get a stable solution for the variational model.

3.2 Remark on imaging formation

Note that another imaging formation pipeline could be:

$$\mathbf{f} = \mathbf{H}\mathbf{w}\mathbf{v} + \mathbf{b}, \quad (3.3)$$

where again \mathbf{v} is multiplicative noise and \mathbf{b} is Gaussian noise. This imaging system will lead to a non-separable variational model which is rather hard to handle. It is interesting to point out that numerically, we observe that our model (3.2) also works rather well for this system. We think that the reason might be as follows. In the multiplicative noise settings, Gaussian additive noise presented in (3.3) could be considered as negligible (see [12]). Moreover, as Gaussian noise in any direction is still Gaussian, roughly speaking, the distribution of $\frac{\mathbf{b}}{\mathbf{v}}$ can be approximated by another Gaussian distribution \mathbf{b}' . Hence, one can rewrite $\mathbf{H}\mathbf{w}\mathbf{v} + \mathbf{b}$ as $(\mathbf{H}\mathbf{w} + \mathbf{b}')\mathbf{v}$. That is to say, (3.3) can be regarded as a special case of (3.1).

3.3 The MAP analysis

Now, let us present some discussion from the point of the MAP analysis. In order to derive a variational model from (3.1), let's introduce an intermediate image:

$$\mathbf{u} = \mathbf{H}\mathbf{w} + \mathbf{b},$$

which can be regarded as a convolution image with Gaussian noise. By this, the image formation mechanism in (3.1) can be rewritten as:

$$\mathbf{f} = \mathbf{u}\mathbf{v}, \quad \mathbf{u} = \mathbf{H}\mathbf{w} + \mathbf{b}. \quad (3.4)$$

Denote $p(x)$ as the probability of variable x and $p(x|y)$ the probability of x on observation y . Using Bayes rules, we can calculate the post-posterior probability:

$$\begin{aligned} p(\mathbf{u}, \mathbf{w} | \mathbf{f}) &= \frac{p(\mathbf{u}, \mathbf{w})p(\mathbf{f} | \mathbf{u}, \mathbf{w})}{p(\mathbf{f})} \\ &= \frac{p(\mathbf{w})p(\mathbf{u} | \mathbf{w})p(\mathbf{f} | \mathbf{u}, \mathbf{w})}{p(\mathbf{f})} \\ &= \frac{p(\mathbf{w})p(\mathbf{u} | \mathbf{w})p(\mathbf{f} | \mathbf{u})}{p(\mathbf{f})}. \end{aligned}$$

Note that here we use the fact $p(\mathbf{f} | \mathbf{u}, \mathbf{w}) = p(\mathbf{f} | \mathbf{u})$ which is due to (3.4).

Now let \mathbf{w} follow Gibbs prior $\frac{e^{-\phi(\mathbf{w})}}{Z}$ where Z is a normalization constant. We have:

$$p(\mathbf{u} | \mathbf{w}) = \frac{1}{\sqrt{2\pi}\sigma} e^{-\frac{\|\mathbf{H}\mathbf{w} - \mathbf{u}\|^2}{2\sigma^2}}.$$

The calculation of $p(\mathbf{f}|\mathbf{u})$ is the same as AA model in [2]. Therefore, the maximization of $p(\mathbf{u}, \mathbf{w}|\mathbf{f})$ leads to:

$$\min_{\mathbf{u}>0, \mathbf{w}} \sum_{i=1}^{mn} \left(\log[\mathbf{u}]_i + \frac{[\mathbf{f}]_i}{[\mathbf{u}]_i} \right) + \frac{\|\mathbf{H}\mathbf{w} - \mathbf{u}\|^2}{2\sigma^2} + \lambda\phi(\mathbf{w}). \tag{3.5}$$

Note that the above MAP framework also works for other type of noises. For instance, if we suppose that v follows Rayleigh distribution which is a rather common assumption for speckle noise, then the objective function should be change as:

$$\min_{\mathbf{u}>0, \mathbf{w}} \sum_{i=1}^{mn} \left(\log[\mathbf{u}]_i + \frac{1}{2\theta^2} \frac{[\mathbf{f}]_i^2}{[\mathbf{u}]_i^2} \right) + \frac{\|\mathbf{H}\mathbf{w} - \mathbf{u}\|^2}{2\sigma^2} + \lambda\phi(\mathbf{w}),$$

since the Rayleigh probability density function is:

$$p(x;\theta) = \frac{x}{\theta^2} \exp\left(-\frac{x^2}{2\theta^2}\right), \quad x \in [0, +\infty).$$

Similarly, if v follows Gaussian distribution with mean 1 and standard variance θ , then the corresponding variational model is:

$$\min_{\mathbf{u}>0, \mathbf{w}} \frac{1}{2\theta^2} \sum_{i=1}^{mn} \left(\frac{[\mathbf{f}]_i}{[\mathbf{u}]_i} - 1 \right)^2 + \frac{\|\mathbf{H}\mathbf{w} - \mathbf{u}\|^2}{2\sigma^2} + \lambda\phi(\mathbf{w}).$$

Let us mention that the techniques in this paper work directly for Rayleigh case. For the Gaussian case, it remains open.

3.4 Basic properties

Evidently, the model (3.2) is more general than the ROL-I and AA model as we accept small tolerance of Gaussian noise. Moreover, if we suppose that σ is small enough, then the new model is component-wise convex.

Proposition 3.1. The problem (3.5) is component-wise convex if $0 < \sigma \leq 2\inf \mathbf{f}$.

Proof. Denote

$$E(\mathbf{u}, \mathbf{w}) := \sum_{i=1}^{mn} \left(\log[\mathbf{u}]_i + \frac{[\mathbf{f}]_i}{[\mathbf{u}]_i} \right) + \frac{\|\mathbf{H}\mathbf{w} - \mathbf{u}\|^2}{2\sigma^2}.$$

The convex on \mathbf{w} is obvious. Moreover, we have:

$$\frac{\partial^2 E}{\partial \mathbf{u}^2} = -\frac{1}{\mathbf{u}^2} + \frac{2\mathbf{f}}{\mathbf{u}^3} + \frac{1}{\sigma^2}.$$

When $\mathbf{u} \in (0, 2\mathbf{f}]$, it is convex; when $\mathbf{u} \in [\sigma, +\infty)$, it is also convex. However, as $\sigma \leq 2\inf \mathbf{f}$, it is convex for all $\mathbf{u} \in (0, +\infty)$. □

In [2], the authors proved the maximum principle for (2.1) when H is the identify operator and $\phi(\cdot) = TV(\cdot)$. We have some similar observation for (3.5).

Proposition 3.2. Suppose that $H \geq 0$ and $H\mathbf{1} = \mathbf{1}$ where $\mathbf{1}$ is constant image with entries 1. Taking $\phi(\cdot) = TV(\cdot)$, denote (u, w) as the solution of problem (3.5).

1. We have:

$$\min(\inf w, \inf f) \leq u \leq \max(\sup w, \sup f).$$

2. If $H = Id$, then:

$$\inf w \geq \inf u \geq \inf f, \quad \sup w \leq \sup u \leq \sup f.$$

Proof. Recall that $\inf f > 0$. For any i fixed, as the function

$$t \rightarrow \log t + \frac{[f]_i}{t} + \frac{|[Hw]_i - t|^2}{2\sigma^2}$$

is monotone decreasing when $t \in (0, \min([f]_i, [Hw]_i))$, we know that:

$$[u]_i \geq \min([f]_i, [Hw]_i).$$

This means:

$$u \geq \min(\inf Hw, \inf f).$$

Using the fact that $H \geq 0$ and for each i fixed, $\sum_j [H]_{i,j} = 1$, we have:

$$[Hw]_i = \sum_j [H]_{i,j} w_j \geq \sum_j [H]_{i,j} (\inf w) = \inf w.$$

This is to say:

$$\inf Hw \geq \inf w.$$

Overall, we obtain the left side of first assertion. By using the same argument, we have the right side.

Now suppose that $H = Id$ and consider:

$$\min \frac{\|w - u\|^2}{2\sigma^2} + \lambda \phi(w), \tag{3.6}$$

with u fixed and $\phi(w) = TV(w)$.

Denote $\beta = \inf w$ and let $w_0 = \max(w, \beta)$. Using the property of $TV(\cdot)$ (see Lemma 1, Section 4.3 of [17]), we know that:

$$TV(w_0) \leq TV(w). \tag{3.7}$$

Moreover, for each i fixed, by the definition of w_0 , we have either:

$$[w_0]_i = [w]_i \quad \text{or} \quad [w_0]_i = \beta \geq [w]_i.$$

As $[u]_i \geq \beta$, both cases lead to:

$$([w_0]_i - [w]_i)([w_0]_i + [w]_i - 2[u]_i) \leq 0.$$

The vector form gives:

$$\|w_0 - u\|^2 \leq \|w - u\|^2.$$

Together with (3.7), we can see that: the replacing of w by w_0 will decrease the objective function value of (3.6). This implies that:

$$\inf w \geq \beta = \inf u.$$

Combining with the fact that:

$$\inf u \geq \min(\inf w, \inf f),$$

we immediately have:

$$\inf u \geq \inf f.$$

This finishes the proof of left part of the second assertion. With the same argument, the rest part is also true. \square

Note that the condition $H \geq 0$ and for each i , $H\mathbf{1} = \mathbf{1}$ is classical in the domain of image processing. We also remark that the above proposition also holds in the continuous settings. The same as in [2], the case with general H remains open.

Proposition 3.3. Suppose that $\phi(\cdot) \geq 0$. Denoting (u, w) as the solution of problem (3.5), then there exist positive constants c_1, c_2 such that

$$c_1 \leq \frac{u}{f} \leq c_2.$$

Proof. Denote the objective function in (3.5) as $E_0(u, w)$. As $\phi(\cdot) \geq 0$, evidently we have:

$$\sum_{i=1}^{mn} \left(\log[u]_i + \frac{[f]_i}{[u]_i} \right) \leq E_0(u, w) \leq E_0(f, \mathbf{0}).$$

Fixing j , for each i , as the minimal point of the function:

$$t \mapsto \log t + \frac{[f]_i}{t},$$

is $t_0 = [f]_i$, we then know that:

$$\log[u]_j + \frac{[f]_j}{[u]_j} + \sum_{i \neq j} \left(\log[f]_i + \frac{[f]_i}{[f]_i} \right) \leq E_0(f, \mathbf{0}).$$

Denoting t as $\frac{[u]_j}{[f]_j}$. Simplifying the above formula, we have:

$$\log t + \frac{1}{t} \leq c_0, \quad (3.8)$$

where

$$c_0 = 1 + \frac{\|f\|^2}{2\sigma^2} + \phi(\mathbf{0}).$$

As $c_0 > 1$, it is easy to know that the below Eq. (3.9) has two positive solutions:

$$\log x + \frac{1}{x} = c_0. \quad (3.9)$$

Denote the left solution as $K_{-1}(c_0)$, and the right one as $c_2 = K_1(c_0)$. From (3.8), we can get:

$$0 < K_{-1}(c_0) \leq t \leq K_1(c_0).$$

As this is for any $t = \frac{[u]_j}{[f]_j}$, we know that:

$$K_{-1}(c_0) \leq \frac{u}{f} \leq K_1(c_0).$$

This finishes the proof by taking $c_1 = K_{-1}(c_0)$, $c_2 = K_1(c_0)$. \square

Let us remark that the above bounds c_1, c_2 are independent of \mathbf{H} . Evidently, the numbers $K_{-1}(c_0)$ and $K_1(c_0)$ which are solutions of Eq. (3.9) should be strongly related to the Lambert W function (see [11]). The latter is also called the Omega function or product logarithm, and is a set of functions, namely the branches of the inverse relation of the function

$$h(z) = ze^z,$$

where z is any complex number.

Moreover, by Proposition 3.3, we immediately have:

$$u \geq K_{-1}(c_0) \inf f > 0, \quad (3.10)$$

thought we should be careful that the factor $K_{-1}(c_0) > 0$ here is rather small since σ is small, and c_0 is big. Anyway, the importance of (3.10) is that the unpleasant restriction $u > 0$ in (3.5) can be replaced by a close condition $u \geq \epsilon$ where ϵ is a known small positive number.

4 Convex relaxation model

Let's examine the model (3.5). Typically, the term $\|w\|_{TV}$ is convex. The above model is very difficult to handle due to the non-convexity of the term $\log u$. We are interested in a convex relaxation model which has smaller non-convexity.

4.1 Convex relaxation technique

Let's present a simple idea to relax the shortcoming of non-convexity. Indeed, it is easy to verify that:

$$g(\mathbf{u}) := \sum_{i=1}^{mn} [u]_i \log [u]_i,$$

is convex. As (3.5) is coercive (see Proposition 3.3), it does not matter if we restrict our \mathbf{u} on some low-bounded region:

$$\{\mathbf{u} : A + \log \mathbf{u} \geq 0\},$$

where A is some constant. Inspired by Proposition 3.2, in practice we find that roughly taking $A \geq -\log(\inf f)$ has been already ok. Moreover, observing that:

$$\log u + A = \frac{u(\log u + A)}{u},$$

and using the decouple idea which is common technique in nowadays image processing domain, we should consider:

$$\min_{\{(u,w,x) : u \geq e^{-A}, x \geq 0\}} \alpha \|\mathbf{x} - \mathbf{u}\|^2 + \sum_{i=1}^{mn} \left(\frac{[u]_i(\log [u]_i + A)}{[x]_i} + \frac{[f]_i}{[u]_i} \right) + \frac{\|\mathbf{H}\mathbf{w} - \mathbf{u}\|^2}{2\sigma^2} + \phi(w). \quad (4.1)$$

The above model is convex if we fix \mathbf{x} . In practice, if we assume that the pixel value region $\mathbf{u} \in [1, 255]$, we can then take $A = 0$ and the condition is thus $\mathbf{u} \geq 1$. The small gap between here with (3.10) usually would not affect the restoration quality significantly.

Moreover, the benefit of using (4.1) instead of (3.5) is that the convex relation technique here is useful to reduce the non-convexity of the objective function. Indeed, let us define, for $\mathbf{u} \geq 1$,

$$g_\alpha(\mathbf{u}) := \min_x \alpha \|\mathbf{x} - \mathbf{u}\|^2 + \sum_{i=1}^{mn} \frac{[u]_i \log [u]_i}{[x]_i}. \quad (4.2)$$

Note that $g_0(\mathbf{u}) = 0$ and $g_{+\infty}(\mathbf{u}) = \sum_i \log [u]_i$. Hence, the function $g_\alpha(\mathbf{u})$ (with $\alpha \in (0, +\infty)$) can be regarded as a trade-off between the non-convex one and a convex one and the replacing of $\sum_i \log [u]_i$ by $g_\alpha(\mathbf{u})$ thus reduces the non-convexity. The selection of α need a balance: the bigger α , the more correct of the statistics of the multiplicative noise nature; the smaller α , the better convexity of the objective function in (4.1) which leads to better stability. Interestingly, we numerically observe that the solution of (4.1) with a rather small α is much more stable than (3.5) and also has rather good restoration quality.

4.2 Analysis on the convex relation technique

The model (4.1) can be solved via the classical alternating minimization method. Define

$$\mathbf{x}^*(\mathbf{u}) := \operatorname{argmin}_x g_\alpha(\mathbf{u}),$$

where $g_\alpha(\mathbf{u})$ is given in (4.2). Readily, we can derive that \mathbf{x}^* is unique and:

$$\mathbf{x}^* \in \left(\mathbf{u}, \mathbf{u} + \sqrt{\frac{\log \mathbf{u}}{\alpha}} \right).$$

For fixed \mathbf{u} , we can find $\mathbf{x}^*(\mathbf{u})$ by solving a cubic equation. This can be done efficiently by Newton method or explicit formula. Define the relative error as:

$$R_\alpha(\mathbf{u}) := \frac{\mathbf{x}^*(\mathbf{u}) - \mathbf{u}}{\mathbf{u}}.$$

Assume that \mathbf{u} is uniformly distributed on $[1, 255]$. Taking $\alpha = 0.02$, with the help of computer simulation, easily we can get:

$$\mathbb{E}(R_\alpha) := \frac{1}{255} \sum_{u=1}^{255} R_\alpha(\mathbf{u}) = 0.004814.$$

Note that for $\alpha = 0.05$, we have $\mathbb{E}(R_\alpha) = 0.002079$. It is even small. Hence, the relative error is negligible and the replacing of (3.5) by (4.1) is reasonable even α is small. This observation is important since smaller α provides better convexity.

4.3 Alternating minimization method

Let us consider to rewrite (4.1) as

$$\min_{\{(u,w,x): u \geq 1, x \geq 0\}} \alpha \|\mathbf{x} - \mathbf{u}\|^2 + \sum_{i=1}^{mn} \left(\frac{[\mathbf{u}]_i (\log [\mathbf{u}]_i)}{[\mathbf{x}]_i} + \frac{[\mathbf{f}]_i}{[\mathbf{u}]_i} \right) + \frac{\|\mathbf{H}\mathbf{w} - \mathbf{u}\|^2}{2\sigma^2} + \phi(\mathbf{w}). \tag{4.3}$$

In this paper, we propose to use an alternating minimization algorithm to solve it and evidently, other modern optimization techniques are also possible. Starting from an initial guess $\mathbf{u}^{(0)}$, the alternating minimization method computes a sequence of iterates

$$\mathbf{w}^{(1)}, \mathbf{x}^{(1)}, \mathbf{u}^{(1)}, \mathbf{w}^{(2)}, \mathbf{x}^{(2)}, \mathbf{u}^{(2)}, \dots, \mathbf{w}^{(k)}, \mathbf{x}^{(k)}, \mathbf{u}^{(k)}, \dots$$

such that

$$\begin{cases} \mathbf{w}^{(k+1)} = \operatorname{argmin}_w \frac{\|\mathbf{H}\mathbf{w} - \mathbf{u}^k\|^2}{2\sigma^2} + \phi(\mathbf{w}), \\ \mathbf{x}^{(k+1)} = \operatorname{argmin}_{\mathbf{x} \geq 0} \alpha \|\mathbf{x} - \mathbf{u}^k\|^2 + \sum_{i=1}^{mn} \left(\frac{[\mathbf{u}^k]_i (\log [\mathbf{u}^k]_i)}{[\mathbf{x}]_i} \right), \\ \mathbf{u}^{(k+1)} = \operatorname{argmin}_{\mathbf{u} \geq 1} \alpha \|\mathbf{x}^{k+1} - \mathbf{u}\|^2 + \sum_{i=1}^{mn} \left(\frac{[\mathbf{u}]_i (\log [\mathbf{u}]_i + A)}{[\mathbf{x}^{k+1}]_i} + \frac{[\mathbf{f}]_i}{[\mathbf{u}]_i} \right) + \frac{\|\mathbf{H}\mathbf{w}^{k+1} - \mathbf{u}\|^2}{2\sigma^2}, \end{cases} \tag{4.4}$$

for $k = 0, 1, 2, \dots$. Denote the above three operators as:

$$\mathbf{w}^{(k+1)} := \mathcal{R}(\mathbf{u}^{(k)}), \quad \mathbf{x}^{(k+1)} := \mathcal{S}(\mathbf{u}^{(k)}), \quad \mathbf{u}^{(k+1)} := \mathcal{T}(\mathbf{w}^{(k+1)}, \mathbf{x}^{(k+1)}),$$

we can express the following relationship between $\mathbf{u}^{(k+1)}$ and $\mathbf{u}^{(k)}$:

$$\mathbf{u}^{(k+1)} = \mathcal{T}(\mathcal{R}(\mathbf{u}^{(k)}), \mathcal{S}(\mathbf{u}^{(k)})), \quad k=0,1,2,\dots.$$

Let us first study the computational cost of the alternating minimization algorithm.

The computation of \mathcal{R} strongly depends on the choice of ϕ . In this paper, we consider:

$$\phi(\mathbf{w}) := \min_x \lambda TV(\mathbf{x}) + \beta \|\mathbf{w} - \mathbf{x}\|^2,$$

where λ, β are positive. Then \mathcal{R} can be calculated via alternating minimization method (see [16] for details).

The computation of \mathcal{S} has closed form. The computation of \mathcal{T} is also not difficult. Note that we can use projection method to handle the constraints $\mathbf{u} \geq 1, \mathbf{x} \geq 0$ in the above minimization procedures.

Again, the convergence of the algorithm is natural in the sense of objective function. Indeed, in every step of the minimization approach (see (4.4)), the objective function value in (4.3) decreases. Then it will converge to a local minimizer of the energy function. Moreover, as the objective function is nearly convex, we numerically observe that the minimizer is rather stable especially when α is rather small.

5 Numerical results

In this section, numerical simulations are performed to validate the efficiency of the proposed method for deblurring and multiplicative noise removal simultaneously. The images "Lena", "Rice", "Earth from space" and "Moon surface" are used in our experiments and the original images are shown in Fig. 2. The pixel values of these images are located in the range [1, 255], so value A in model (4.1) is selected to be 0 in all experiments. In addition, in the experiments, the peak signal noise ratio (PSNR) and the relative error (ReEr) are used to show the restoring quality of the recovered images quantitatively. Suppose that the image size is m -by- n , PSNR value is defined as follows:

$$\text{PSNR} = 10 \log_{10} \left(\frac{V^2}{\text{MSE}} \right),$$

where $\text{MSE} = \sum_{i=1}^m \sum_{j=1}^n (\tilde{\mathbf{w}}(i,j) - \mathbf{w}(i,j))^2 / mn$, $\mathbf{w}, \tilde{\mathbf{w}}$ are the original image and the recovered image respectively, and $V = \max_{i,j}(\tilde{\mathbf{w}}(i,j), \mathbf{w}(i,j))$. With the same meanings of \mathbf{w} and $\tilde{\mathbf{w}}$ in the definition of PSNR, the relative error of the recovered image $\tilde{\mathbf{w}}$ is defined as

$$\text{ReEr} = \frac{\|\tilde{\mathbf{w}} - \mathbf{w}\|^2}{\|\mathbf{w}\|^2}.$$

The stopping criterion for the experiments by the proposed method is that the relative difference between the successive iterates of the restored images should satisfy the following inequality:

$$\frac{\|\tilde{\mathbf{w}}^{(i+1)} - \tilde{\mathbf{w}}^{(i)}\|_2}{\|\tilde{\mathbf{w}}^{(i+1)}\|_2} < 10^{-3}.$$

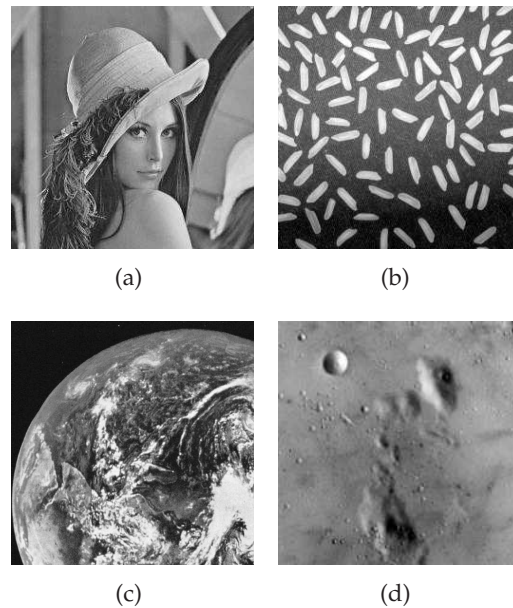


Figure 2: (a) The original "Lena" image; (b) the original "Rice" image; (c) the reference "Earth from space" image; (d) the reference "Moon surface" image.

In all experiments, the initial guess in the alternating iterative algorithm is set to be the observed image. All codes are written in MATLAB 7.0 and all experiments are implemented on a personal computer with 2.80GHz central processing unit and 2.0G memory.

In the experiments, the multiplicative noise v appearing in (3.1) or (3.3) is a Gamma noise γ or a Gaussian noise η , the mean value of both random noises is one. Their probability density function are given by

$$p_{\text{Gam}}(\gamma; L) = \begin{cases} \frac{L^L \gamma^{L-1}}{\Gamma(L)} e^{-L\gamma}, & \gamma > 0, \\ 0, & \gamma \leq 0, \end{cases} \quad (5.1)$$

and

$$p_{\text{Gaus}}(\eta; \sigma) = \begin{cases} \frac{1}{\sqrt{2\pi}\sigma} e^{-\frac{(\eta-1)^2}{2\sigma^2}}, & \eta > 0, \\ 0, & \eta \leq 0, \end{cases} \quad (5.2)$$

respectively. The level of the Gamma noise γ with the fixed mean value is determined by the parameter L since the variance of γ equals the reciprocal value of L . Here σ in (5.2) is the standard variance of the Gaussian noise η , the larger σ is, the more serious the Gaussian noise is. The parameter α in (4.1) is set to be 0.05 in all experiments.

The following six experiments have been completed to show the effectiveness of the proposed method.

5.1 Experiment 1

In the first experiment, the original “Lena” image is blurred by Gaussian blur, motion blur, average blur and defocus blur respectively, and then a small Gaussian noise with standard variance(std) 1 is added, after that, the resulting images are further corrupted by a multiplicative Gamma noise with variance 0.01, the degraded images are shown in Figs. 3-6 (a). Figs. 3-6 (b) show the recovered images corresponding to (a) in each figure and we can see both the blur and Gamma noise are removed efficiently in each restoration. The relative errors of the degraded images and the relative errors, PSNRs of the recovered images and computing times of the restorations are shown in Table 1. The figures and the table clearly show that the proposed model (4.1) is very effective to remove different kinds blurs and multiplicative noise simultaneously.

Table 1: The recovered results for Experiment 1.

blurs	Observed	Recovered		
	ReEr	ReEr	PSNR	Time(s)
Gaussian	0.1376	0.0912	26.6	69.1
Motion	0.1713	0.0880	26.8	106.8
Average	0.1438	0.0934	26.3	72.2
Defocus	0.1307	0.0844	27.1	75.1

5.2 Experiment 2

In this experiment, larger Gaussian noise is imposed on the degradations. That is, Gaussian noise with a larger std appears in model (3.1). In our simulations, Gaussian noises with std 5 and 10 are added to the blurred “Lena” image respectively. And then a multiplicative Gamma noise with variance 0.01 is added. The degraded images and the corresponding recovered images are shown in Fig. 7 and Fig. 8 respectively. The relative errors of the degraded images and the relative errors, PSNRs of the recovered images and computing times of the restorations are shown in Table 2. These two figures and this table demonstrate that the proposed model (4.1) is very effective to remove blurs and multiplicative noise in model (3.1) with large Gaussian noise.

Table 2: The recovered results for Experiment 2.

std	Observed	Recovered		
	ReEr	ReEr	PSNR	Time(s)
5	0.1424	0.0907	26.5	67.6
10	0.1566	0.0933	26.3	73.4

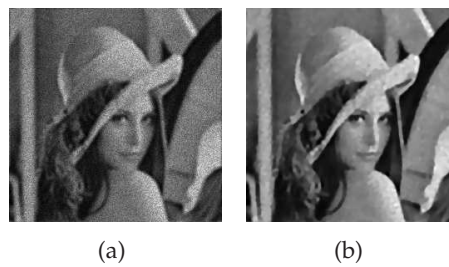


Figure 3: (a) The original "Lena" image is blurred by Gaussian blur `fspecial('gaussian',5,2)` and then a Gaussian noise with standard variance 1 is added, after that, it is further corrupted by Gamma noise with variance 0.01; (b) the recovered image by the proposed model (4.1).



Figure 4: (a) The original "Lena" image is blurred by motion blur `fspecial('motion',5)` and then a Gaussian noise with standard variance 1 is added, after that, it is further corrupted by Gamma noise with variance 0.01; (b) the recovered image by the proposed model (4.1).

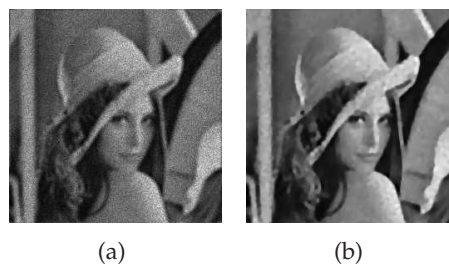


Figure 5: (a) The original "Lena" image is blurred by average blur `fspecial('average',5)` and then a Gaussian noise with standard variance 1 is added, after that, it is further corrupted by Gamma noise with variance 0.01; (b) the recovered image by the proposed model (4.1).



Figure 6: (a) The original "Lena" image is blurred by Defocus blur `fspecial('disk',2)` and then a Gaussian noise with standard variance 1 is added, after that, it is further corrupted by Gamma noise with variance 0.01; (b) the recovered image by the proposed model (4.1).



Figure 7: (a) The original "Lena" image is blurred by Gaussian blur $f_{\text{special}}('gaussian',5,2)$ and then a Gaussian noise with standard variance 5 is added, after that, it is further corrupted by Gamma noise with variance 0.01; (b) the recovered image by the proposed model (4.1).



Figure 8: (a) The original "Lena" image is blurred by Gaussian blur $f_{\text{special}}('gaussian',5,2)$ and then a Gaussian noise with standard variance 10 is added, after that, it is further corrupted by Gamma noise with variance 0.01; (b) the recovered image by the proposed model (4.1).

5.3 Experiment 3

In this experiment, we show the restoring results of the images corrupted by serious blurs and multiplicative Gamma noise with different levels. Since no Gaussian noise is added in this experiment, the degradation model is same as the one in (1.2) and it is the pure problem just only for blur and multiplicative noise removal. Therefore, we compare our results with those obtained by RLO-I method (2.2) and AA method (2.1). The stopping criteria for the latter two methods is that the iteration number achieves 1000 steps. Figs. 9-12 show the results when the original images "Rice" is blurred by Gaussian blur and then corrupted by multiplicative noise with variance 0.01; "Lena" is blurred by Motion blur and then corrupted by multiplicative noise with variance 0.01; "Rice" is blurred by Gaussian blur and then corrupted by multiplicative noise with variance 0.03; "Lena" is blurred by Motion blur and then corrupted by multiplicative noise with variance 0.03. From the recovered quantities shown in Tables 3-4, we can judge the recovered PSNRs and relative errors by the proposed method are much better than those obtained by RLO-I method and AA method. Furthermore, longer calculating times are required in the latter two methods. In addition, the deblurring effect by the proposed method is superior to that by RLO-I method and AA method in terms of recovering visual effect. For example, in Fig. 12, the small trace of motion blur is still obvious in images (e) and (f) recovered by

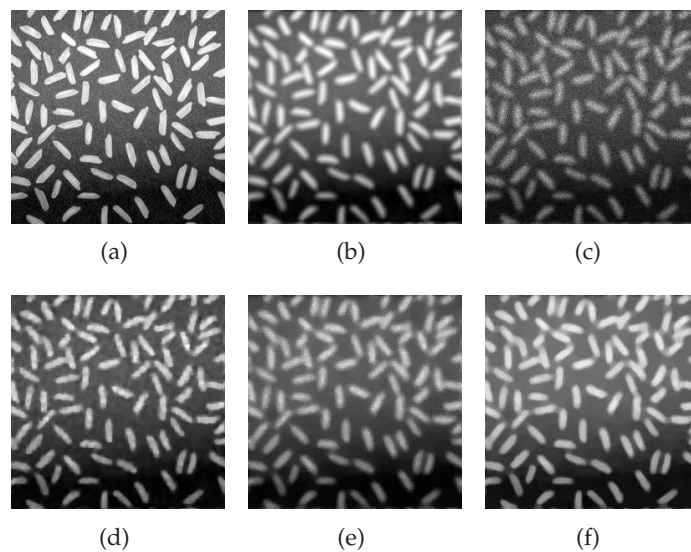


Figure 9: (a) The original "Rice" image; (b) (a) is blurred by Gaussian blur `fspecial('gaussian',7,5)` and no Gaussian noise is added; (c) (b) further corrupted by Gamma noise with variance 0.01; (d) the recovered image by the proposed model (4.1); (e) the recovered image by RLO-I; (f) the recovered image by AA.



Figure 10: (a) The original "Lena" image; (b) (a) is blurred by motion blur `fspecial('motion',7)` and no Gaussian noise is added; (c) (b) further corrupted by Gamma noise with variance 0.01; (d) the recovered image by the proposed model (4.1); (e) the recovered image by RLO-I; (f) the recovered image by AA.

RLO-I method and AA method respectively, but the blur is more faint in the recovered image (d) by the proposed method. On the other hand, the recovered images by RLO-I method and AA method are smooth so that the deblurred result is not so obvious. So,

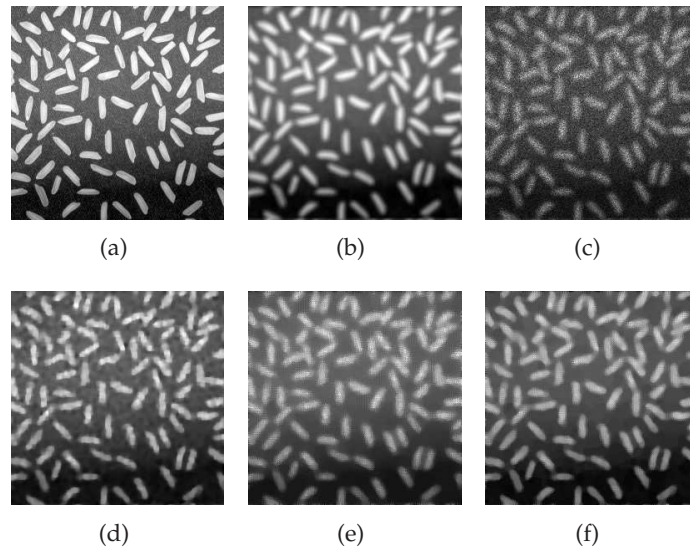


Figure 11: (a) The original "Rice" image; (b) (a) is blurred by Gaussian blur `fspecial('gaussian',7,5)` and no Gaussian noise is added; (c) (b) further corrupted by Gamma noise with variance 0.03; (d) the recovered image by the proposed model (4.1); (e) the recovered image by RLO-I; (f) the recovered image by AA.



Figure 12: (a) The original "Lena" image; (b) (a) is blurred by Gaussian blur `fspecial('motion',7)` and no Gaussian noise is added; (c) (b) further corrupted by Gamma noise with variance 0.03; (d) the recovered image by the proposed model (4.1); (e) the recovered image by RLO-I; (f) the recovered image by AA.

comparing to RLO-I method and AA method, we conclude that the proposed method converges fast and can remove blurs and multiplicative noises simultaneously efficiently, even both the blur and multiplicative noise are serious.

Table 3: The recovered results for Experiment 3 when the variance of Gamma noise is 0.01.

images	method	Observed	Recovered		
		ReEr	ReEr	PSNR	Time(s)
"Rice"	Proposed	0.1636	0.1034	25.3	51.2
	RLO-I	0.1636	0.1526	21.6	146.2
	AA	0.1636	0.1257	22.7	157.5
"Lena"	Proposed	0.1930	0.0971	25.9	91.9
	RLO-I	0.1930	0.1651	21.3	135.6
	AA	0.1930	0.1150	24.7	146.8

Table 4: The recovered results for Experiment 3 when the variance of Gamma noise is 0.03.

images	method	Observed	Recovered		
		ReEr	ReEr	PSNR	Time(s)
"Rice"	Proposed	0.2145	0.1179	24.3	82.9
	RLO-I	0.2145	0.1654	22.3	120.0
	AA	0.2145	0.1336	23.3	156.3
"Lena"	Proposed	0.2386	0.1096	24.9	109.0
	RLO-I	0.2386	0.1707	21.0	134.9
	AA	0.2386	0.1178	24.2	146.4

5.4 Experiment 4

The aerial image "Earth from space" is used to implement the numerical results in this experiment. Figs. 13-14 show the recovered results under different degradation conditions. The recovered quantities show in Table 5. These figures and Table 5 tell us that the recovered images by RLO-I method and AA method are more smooth. But the proposed method is also very effective for the restoration of aerial images.

Table 5: The recovered results for Experiment 4.

std	method	Observed	Recovered		
		ReEr	ReEr	PSNR	Time(s)
1	Proposed	0.1175	0.0734	29.3	297.9
0	Proposed	0.1978	0.0994	26.6	260.1
	RLO-I	0.1978	0.1200	25.0	543.1
	AA	0.1978	0.1078	25.9	573.5

5.5 Experiment 5

The formulation (4.1) is derived for removing multiplicative Gamma noise, and the above four experiments are all performed for Gamma noise removal. In this experiment, we give some tests to demonstrate that the proposed model is also very useful to remove blurs and multiplicative Gaussian noise simultaneously. The image "Moon surface" is

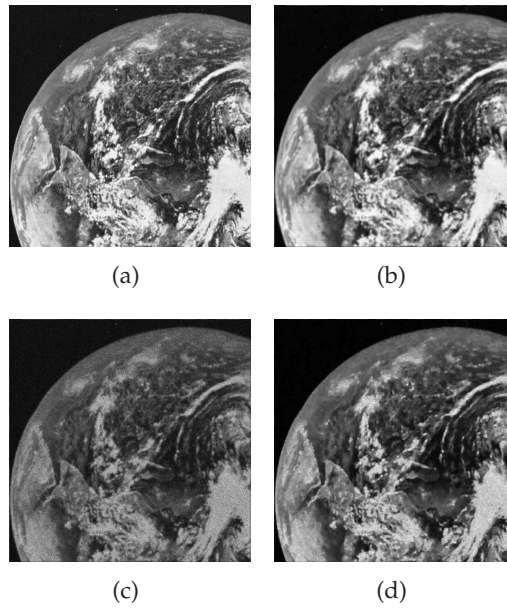


Figure 13: (a) The reference “Earth from space” image; (b) (a) is blurred by Defocus blur $f_{\text{special}}('disk', 2)$ and then a Gaussian noise with standard variance 1 is added; (c) (b) is further corrupted by Gamma noise with variance 0.01; (d) the recovered image by the proposed model (4.1).

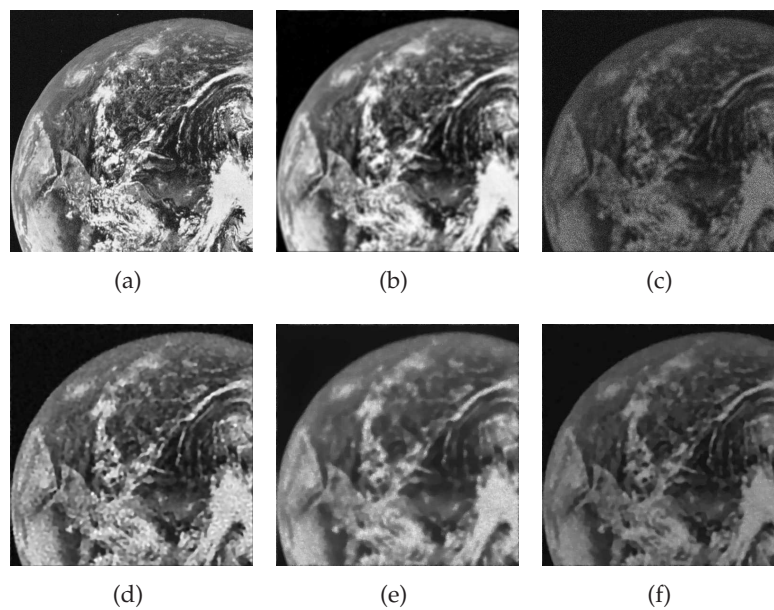


Figure 14: (a) The reference “Earth from space” image; (b) (a) is blurred by Defocus blur $f_{\text{special}}('disk', 4)$ and no Gaussian noise is added; (c) (b) is further corrupted by Gamma noise with variance 0.03; (d) the recovered image by the proposed model (4.1); (d) the recovered image by RLO-I; (e) the recovered image by AA.

used in this experiment, it is blurred by Gaussian blur with std $\sqrt{2}$ first. Then in the first test, the blurred image is further added Gaussian noise and then corrupted by Gaussian multiplicative noise with std 0.2. Which still follows the model (3.1) but the kind of multiplicative noise is Gaussian. The degraded and recovered images are shown in Fig. 15. This test shows that the proposed model (4.1) can also restore images efficiently when the multiplicative noise is Gaussian in (3.1). The second test is to directly corrupt the blurred image by Gaussian multiplicative noise with std 0.2 and no additive Gaussian noise is added. The same experiment appeared in [2, 21], so in the second test, we compare the restored results by RLO-I method and AA method and the recovered images are shown in Fig. 16. This figure and Table 6 clearly show that the proposed method (4.1) is more helpful for the multiplicative Gaussian noise removal in image restorations than both RLO-I method and AA method.

Table 6: The recovered results for Experiment 5.

std	method	Observed	Recovered		
		ReEr	ReEr	PSNR	Time(s)
5	Proposed	0.2130	0.0739	28.4	47.4
0	Proposed	0.2091	0.0721	28.7	40.8
	RLO-I	0.2091	0.0912	26.6	90.2
	AA	0.2091	0.0852	27.7	109.1

5.6 Experiment 6

In this experiment, we apply model (4.1) to test images degraded by (3.3). Three tests corresponding to Figs. 7, 8 and Fig. 15 are performed. That is, in the first test, blurred "Lena" image is corrupted by Gamma noise and then a Gaussian noise with std 5 is added; in the second test, blurred "Lena" image is corrupted by Gamma noise and then a Gaussian noise with std 10 is added; in the third test, blurred "Lena" image is corrupted by Gaussian multiplicative noise and then a Gaussian noise with std 5 is added. The degraded images and corresponding recovered images are shown in Fig. 17 and the recovered quantities are reported in Table 7. It is interesting to note that the PSNRs and the computational times in this experiment are about the same as those recovered results where images are degraded by (3.1) for both Gamma and Gaussian multiplicative noise.

Table 7: The recovered results for Experiment 6.

images	std	Observed	Recovered		
		ReEr	ReEr	PSNR	Time(s)
"Lena"	5	0.1423	0.0906	26.5	72.3
	10	0.1564	0.0932	26.3	71.3
"Moon"	5	0.2128	0.0736	28.5	45.2

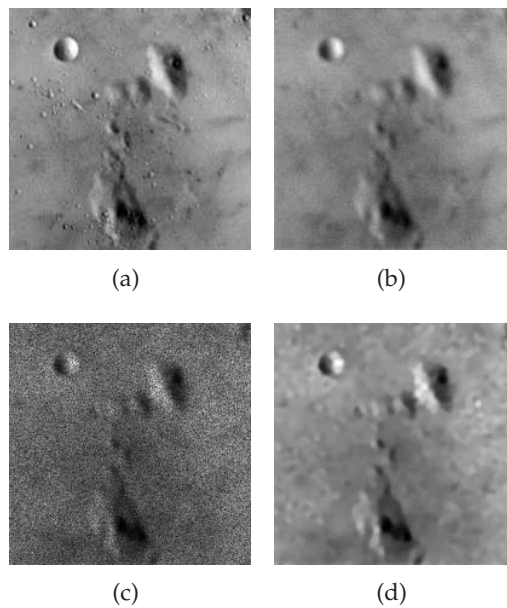


Figure 15: (a) The original "Moon surface" image; (b) (a) is blurred by Gaussian blur `fspecial('gaussian',7,2)` and then a Gaussian noise with standard variance 5 is added; (c) (b) is further corrupted by multiplicative Gaussian noise with standard variance 0.2; (d) the recovered image by the proposed model (4.1).

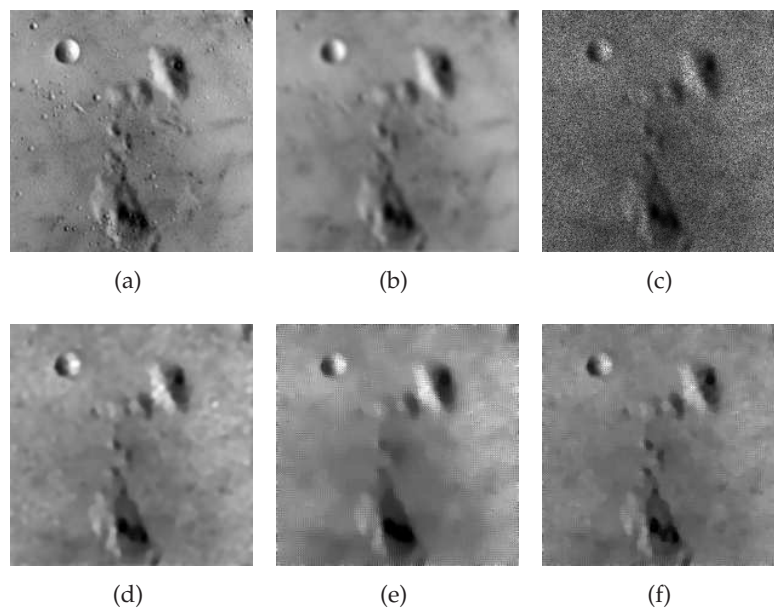


Figure 16: (a) The original "Moon surface" image; (b) (a) is blurred by Gaussian blur `fspecial('gaussian',7,2)` and no Gaussian noise is added; (c) (b) further corrupted by multiplicative Gaussian noise with standard variance 0.2; (d) the recovered image by the proposed model (4.1); (e) the recovered image by RLO-I; (f) the recovered image by AA.

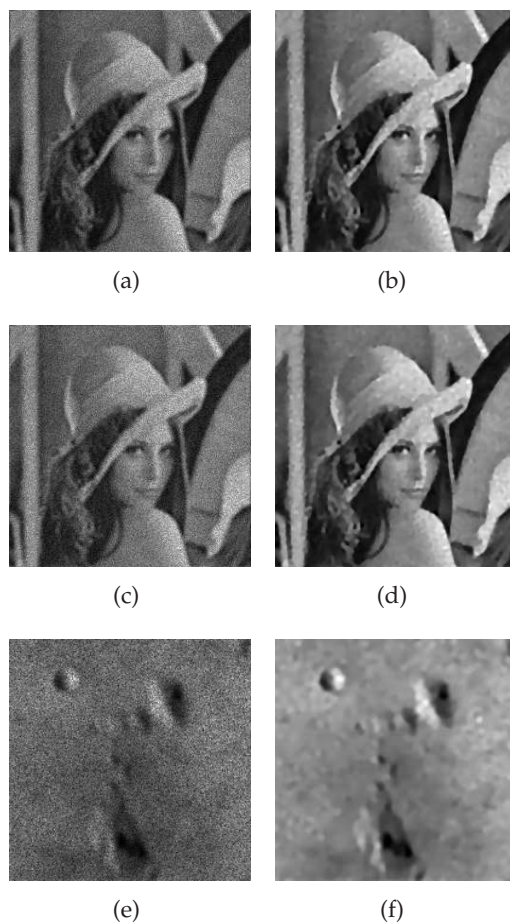


Figure 17: (a) The original “Lena” image is blurred by Gaussian blur `fspecial('gaussian',5,2)`, then it is corrupted by Gamma noise with variance 0.01 and a Gaussian noise with std 5 is added; (b) the recovered image of (a) by (4.1); (c) the “Lena” image is blurred by `fspecial('gaussian',5,2)`, then it is corrupted by Gamma noise with variance 0.01 and a Gaussian noise with std 10 is added; (d) the recovered image of (c) by (4.1); (e) the original “Moon surface” image is blurred by `fspecial('gaussian',7,2)`, then it is further corrupted by multiplicative Gaussian noise with std 0.2 and a Gaussian noise with std 5 is added; (f) the recovered image of (e) by (4.1).

6 Concluding remarks

In this paper, we focus on variational approach to handle the deblurring problem under multiplicative noise. Based on some physical blurring-noisy assumptions, we propose a new variational model for this issue. Some basic properties including the maximal principle are studied for this component-wise convex model. Moreover, as this is still non-convex model, we then propose to approximate it by a convex relaxation model which is a balance between the previous non-convex model and a convex model. As the relaxed model has better convexity, it can be solved by the classical alternating minimization approach which is stable. The convergence in the sense of objective function of this

algorithm is guaranteed. Our experimental results show that the quality of deblurring images by the proposed method is quite promising. The extension of our basic idea in this paper to other non-convex model will also be extremely interesting.

Acknowledgments

This work is supported in part by: Hong Kong RGC 203109, 211710, RGC 211911; the FRGs of Hong Kong Baptist University; and NSFC Grant No. 11101195 and No. 11171371; Specialized Research Fund for the Doctoral Program of Higher Education of China No. 20090211120011; China Postdoctoral Science Foundation funded project No. 2011M501488. The authors would like to thank the extremely helpful comments of the anonymous reviewers and Dr. Dong Yiqiu.

References

- [1] L. Ambrosio, N. Fusco and D. Pallara, *Functions of Bounded Variation and Free Discontinuity Problem*, Oxford university press, 2000.
- [2] G. Aubert and J. Aujol, A variational approach to remove multiplicative noise, *SIAM J. Appl. Math.*, Vol. 68 (2008), pp. 925-946.
- [3] G. Aubert and P. Kornprobst, *Mathematical Problems in Image Processing: Partial Differential Equations and the Calculus of Variations*, second edition ed., Ser. Applied Mathematical Sciences. Springer, Vol. 147 (2006).
- [4] L. Bar, N. Schen and N. Kiryati, Image deblurring in the presence of impulsive noise, *Int. J. Computer Vision*, Vol. 70 (2006), pp. 279-298.
- [5] J. Bioucas-Dias and M. Figueiredo, Total variation restoration of speckled images using a split-bregman algorithm, *Proc. IEEE ICIP 2009*.
- [6] J. Cai, R. Chan and C. Fiore, Minimization of a detail-preserving regularization functional for impulse noise removal, *J. Math. Imaging Vis.*, Vol. 29 (2007), pp. 79-91.
- [7] J. Cai, R. Chan and M. Nikolova, Two-phase approach for deblurring images corrupted by impulse plus Gaussian noise, *Inverse Problems and Imaging*, Vol. 2 (2008), pp. 187-204.
- [8] R. H. Chan, T. F. Chan and C. K. Wong, Cosine transform based preconditioners for total variation deblurring, *IEEE Trans. Image Process.*, vol. 8 (1999), pp. 1472-1478.
- [9] R. Chan and K. Chen, Multilevel algorithm for a Poisson noise removal model with total-variation regularization, *Int. J. Comput. Math.*, Vol. 84 (2007), pp. 1183-1198.
- [10] E. Cole, The removal of unknown image blurs by Homomorphic filtering, Technical Report 0038, Department of Electrical Engineering, University of Toronto, 1973.
- [11] R. M. Corless, G. H. Gonnet, D. E. G. Hare, D. J. Jeffrey and D. E. Knuth, On the Lambert W function, *Advances in Computational Mathematics*(Berlin, New York: Springer-Verlag), Vol. 5 (1996), pp. 329-359.
- [12] S. Durand, J. Fadili and M. Nikolova, Multiplicative noise removal using L1 fidelity on frame coefficients, *J. Math. Imaging Vis.*, Vol. 36 (2010), pp. 201-226.
- [13] J. Hadamard, Sur les problèmes aux dérivées partielles et leur signification physique, *Princeton University Bulletin*, 1902, pp. 49-52.
- [14] Y. Huang, M. Ng and Y. Wen, A new total variation method for multiplicative noise removal, *SIAM J. Imaging Sci.*, Vol. 2 (2009), pp. 20-40.

- [15] Y. Huang, M. Ng and Y. Wen, Fast image restoration methods for impulse and Gaussian noises removal, *IEEE Signal Processing Lett.*, Vol. 16 (2009), pp. 457-460.
- [16] Y. Huang, M. Ng and Y. Wen, A fast total variation minimization method for image restoration, *SIAM Multiscale Model. Simul.*, Vol. 7 (2008), pp. 774-795.
- [17] P. Kornprobst, R. Deriche and G. Aubert, Image sequence analysis via partial differential equations, *J. Math. Imaging Vis.*, Vol. 11 no. 1 (1999), pp. 5-26.
- [18] C. Liu, R. Szeliski, S. Kang, C. Zitnick and W. Freeman, Automatic estimation and removal of noise from a single image, *IEEE Trans. PAMI*, Vol. 30 (2008), pp. 299-314.
- [19] R. Puetter, T. Gosnell and Y. Amos, Digital image reconstruction: deblurring and denoising, *Annual Review of Astronomy & Astrophysics*, Vol. 43 (2005), pp. 139-194.
- [20] T. R. Chartrand and T. Asaki, A variational approach to reconstructing images corrupted by Poisson noise, *J. Math. Imaging Vis.*, Vol. 27 (2007), pp. 257-263.
- [21] L. Rudin, P. Lions and S. Osher, Multiplicative denoising and deblurring: theory and algorithms, In S. Osher and N. Paragios, editors, *Geometric Level Sets in Imaging, Vision, and Graphics*, Springer, 2003, pp. 103-119.
- [22] L. Rudin, S. Osher and E. Fatemi, Nonlinear total variation based noise removal algorithms, *Physica D*, Vol. 60 (1992), pp. 259-268.
- [23] J. Shi and S. Osher, A nonlinear inverse scale method for a convex multiplicative noise model, *SIAM J. Imaging Sci.*, Vol. 1 (2008), pp. 294-321.
- [24] G. Steidl and T. Teuber, Removing multiplicative noise by Douglas-Rachford splitting methods, *J. Math. Imaging Vis.*, vol. 36 (2010), pp. 168-184.
- [25] Y. Tsin, V. Ramesh and T. Kanade, Statistical calibration of CCD imaging process, *Proc. IEEE Eighth Int'l Conf. Computer Vision*, Vol. 1 (2001), pp. 480-487.
- [26] Y. Xiao, T. Zeng, J. Yu and M. Ng, Restoration of images corrupted by mixed Gaussian-impulse noise via l_1 - l_0 minimization, *Pattern Recognition*, Vol. 44 no. 8 (2011), pp. 1708-1728.
- [27] T. Zeng, X. Li and M. Ng, Alternating minimization method for total variation based wavelet shrinkage model, *Communications in Computational Physics*, Vol. 8 no. 5 (2010), pp. 976-994.
- [28] T. Zeng and M. Ng, On the total variation dictionary model, *IEEE Trans. Image Process.*, Vol. 19 no. 3 (2010), pp. 821-825.